# REPORT DOCUMENTATION PAGE

AFRL-SR-BL-TR-01-

0555

Public reporting burden for this collection of information is estimated to average 1 hour per response, including the time for reviewing instructions, searchir ving
the collection of information. Send comments regarding this burden estimate or any other aspect of this collection of information, including suggestic tion
Operations and Reports, 1215 Jefferson Davis Highway, Suite 1204, Arlington, VA 22202-4302, and to the Office of Management and Budget, Paperwol

| 1. AGENCY USE ONLY (Leave blank) | 2. REPORT DATE | 3. REPORT |
|---|---|---|
| | | 01 JULY 1998 - 30 JUNE 2001 |

**4. TITLE AND SUBTITLE**
Accurate Multiresolution Modeling of the Earth's Gravitational Field

**5. FUNDING NUMBERS**
F49620-98-1-0491

**6. AUTHOR(S)**
Dr. G. Beylkin

**7. PERFORMING ORGANIZATION NAME(S) AND ADDRESS(ES)**
Department of Applied Mathematics
University of Colorado
Boulder, CO 80309-0526

20011126 107

**9. SPONSORING/MONITORING AGENCY NAME(S) AND ADDRESS(ES)**
AFOSR/NM
801 N. Randolph Street Room 732
Arlington, VA 22203-1977

**10. SPONSORING/MONITORING AGENCY REPORT NUMBER**
F49620-98-1-0491

**11. SUPPLEMENTARY NOTES**

AIR FORCE OFFICE OF SCIENTIFIC RESEARCH (AFOSR)
NOTICE OF TRANSMITTAL DTIC. THIS TECHNICAL REPORT
HAS BEEN REVIEWED AND IS APPROVED FOR PUBLIC RELEASE
LAW AFR 190-12. DISTRIBUTION IS UNLIMITED.

**12a. DISTRIBUTION AVAILABILITY STATEMENT**
APPROVED FOR PUBLIC RELEASE, DISTRIBUTION UNLIMITED

**13. ABSTRACT** (Maximum 200 words)
The thrust of this project has been two-fold, namely, (1) to improve the performance of existing models of Earth's gravitational field, mainly with respect to speed of evaluation; and (2) to develop new multi resolution estimation techniques to produce new gravitational models. We have constructed two local models of the gravitational field, both of which map the surface of a sphere to the surface of a cube. These models differ in the choice of basis functions. The first uses multi-wavelets to represent the gravitational field at a fixed distance from Earth, and the second mode] uses B-splines. Both models use polynomial interpolation to compute the variation in height of the gravity field. Significant progress has been made towards implementing a procedure for estimating gravity models directly from physical measurements. We have developed a new estimation algorithm, a multi-resolution rank-revealing QR decomposition. This algorithm produces the "minimum detail" solution instead of the usual minimum norm solution of the ill-conditioned least squares problem. A basis for bandlimited functions has been constructed using a new method for computing the generalized Gaussian quadratures for exponentials. These bases are closely related to the prolate spheroidal wave functions, and we plan to create the next generation of models for evaluation and estimation of the gravity field using such bases. These bases are nearly optimal in terms of the number of coefficients necessary to represent a bandlimited function.

**14. SUBJECT TERMS**

**15. NUMBER OF PAGES**
24

**16. PRICE CODE**

| 17. SECURITY CLASSIFICATION OF REPORT | 18. SECURITY CLASSIFICATION OF THIS PAGE | 19. SECURITY CLASSIFICATION OF ABSTRACT | 20. LIMITATION OF ABSTRACT |
|---|---|---|---|

Standard Form 298 (Rev. 2-89) (EG)
Prescribed by ANSI Std. 239.18
Designed using Perform Pro, WHS/DIOR, Oct 94

# Final Report
## September, 2001

## Abstract

The thrust of this project has been two-fold, namely, (1) to improve the performance of existing models of Earth's gravitational field, mainly with respect to speed of evaluation; and (2) to develop new multiresolution estimation techniques to produce new gravitational models.

We have constructed two local models of the gravitational field, both of which map the surface of a sphere to the surface of a cube. These models differ in the choice of basis functions. The first uses multiwavelets to represent the gravitational field at a fixed distance from Earth, and the second model uses B-splines. Both models use polynomial interpolation to compute the variation in height of the gravity field.

Significant progress has been made towards implementing a procedure for estimating gravity models directly from physical measurements. We have developed a new estimation algorithm, a multiresolution rank-revealing QR decomposition. This algorithm produces the "minimum detail" solution instead of the usual minimum norm solution of the ill-conditioned least squares problem.

A basis for bandlimited functions has been constructed using a new method for computing the generalized Gaussian quadratures for exponentials. These bases are closely related to the prolate spheroidal wave functions, and we plan to create the next generation of models for evaluation and estimation of the gravity field using such bases. These bases are nearly optimal in terms of the number of coefficients necessary to represent a bandlimited function.

In addition, we have begun work on a new type of ODE solver (spectral deferred corrections), which will work in conjunction with the new gravity models, and should provide further improvements to speed and accuracy of computing satellite ephemerides.

New gravity models of the type described here were transferred to Space Warfare Command in Colorado Springs.

# 1 Introduction

We recall the form of the spherical harmonic model of the gravitational potential,

$$V(r, \phi, \theta) = \frac{GM}{r} \left\{ 1 + \sum_{n=2}^{N} \left( \frac{R}{r} \right)^n Y_n(\phi, \theta) \right\} , \tag{1}$$

where $GM$ is Earth's gravitational constant, $r$ is the length of the radius vector from Earth's center of mass, $R$ is the radius of the Earth (either equatorial or polar radius), $\phi$ is geocentric longitude and $\theta$ is geocentric latitude. The spherical harmonic $Y_n(\phi, \theta)$ is defined as

$$Y_n(\phi, \theta) = \sum_{m=0}^{n} \overline{P}_n^m (\sin \theta) \left( \overline{C}_n^m \cos m\phi + \overline{S}_n^m \sin m\phi \right) ,$$

where $\overline{C}_n^0, \overline{C}_n^1, \ldots, \overline{C}_n^n, \overline{S}_n^1, \ldots, \overline{S}_n^n$, for $2 \leq n \leq N$ are normalized coefficients, and $\overline{P}_n^m$ is the normalized associated Legendre function of degree $n$ and order $m$. The parameter $N$ in (1), the number of terms retained in the model, determines the order of the model. For example, $N = 41$ corresponds to a 41st order model, and so on. As is well known, (1) is a solution of the Laplace equation in spherical coordinates $(r, \phi, \theta)$, $r > R$

The cost of evaluating $V$ at a point $(r, \phi, \theta)$ via (1) grows rapidly with the number of retained terms. Namely, if $N$ terms are retained in (1) then the number of operations to evaluate $V$ is proportional to $N^2$. Thus, changing the model from that using 20 terms to the model using 200 terms requires roughly 100 times more operations.

We observe that there are several sources of inefficiency in using this representation. First, the functions $(R/r)^n$, $n = 2, 3, \ldots$ are "nearly parallel," which means that the organization of the sum in (1) is not efficient for computing. Second, the functions $Y_n(\phi, \theta)$ are global and thus cannot model the regional variations in the Earth's geopotential with the detail and economy provided by local functions such as splines or wavelets. Unlike global functions, the resolution of local functions can be adjusted to the level required to accurately model local features, a process known as "adaptive sampling."

In what follows we use the terms "local" and "multiresolution" representations. In a local representation the elementary building blocks are basis functions with localized support, e.g. B-splines. These representations typically do not use adaptive sampling; rather, the resolution is uniform throughout the model. Multiresolution representations also use localized basis functions

(e.g. wavelets) but, in addition, can use adaptive sampling to more efficiently accommodate different variability of the geopotential in different regions.

# 2 Local Models of the Gravity Field

Two local models have been developed under this grant, but before describing them it will be advantageous to provide background by describing an earlier model, developed under an earlier grant.

## 2.1 Doubly Periodic B-spline Model

The local model developed under DARPA grant *Efficient Representation of the Earth's Gravitational Field* comprises a set of spherical shells, each corresponding to a fixed value of the radial distance $r$. On each shell, the potential field (or one of its derivatives) is modeled by a doubly periodic B-spline expansion. For purposes of illustration, let $r_0$ be a fixed value of $r$. To model the field on a spherical shell at $r = r_0$ we construct the following representation,

$$V(r_0, \phi, \theta) = \sum_{k=0}^{M-1} \sum_{l=0}^{M-1} s_{k,l}\, \beta(Mx - k)\beta(My - l) \qquad (2)$$

where $2\pi x = \theta$ and $2\pi y = \phi$. In (2), $\beta$ denotes the B-spline (compactly supported, piecewise polynomial function) of sufficiently high order, and $1/M$ is the length of the largest interval on which the spline is a polynomial. The choice of the integer $M$ and the order of the B-splines depends upon accuracy and memory requirements and both are adjustable parameters in the model.

The cost of evaluating the B-spline series (2) is a constant that depends on the order of the spline, and is proportional to $(mdeg + 1)^2$, where $mdeg$ denotes the degree of the spline. Thus, for example, if we use B-splines of degree seven, then roughly sixty-four multiplications are required to evaluate the right-hand side of (2). Note that this cost is independent of the parameter $M$, which instead governs memory storage requirements, with its magnitude being dictated by the required precision. It is obvious from (2) that $M^2$ coefficients must be stored in computer memory for each spherical shell. The values of $M$ and $mdeg$ are in inverse proportion; the larger is $M$, the smaller is $mdeg$, and vice versa, in order to achieve any prescribed accuracy. Thus,

the issue of parameter selection becomes a trade-off between computational speed and computer storage requirements.

Now let us describe how we use (2) to obtain the values of the geopotential and its derivatives at locations *between* the tabulated shells. Suppose that we want to evaluate at a distance $r'$ above the Earth's surface, and that $r_k < r' < r_{k+1}$, where $r_k$ and $r_{k+1}$ correspond to consecutive, tabulated shells. We simply compute the value of the potential on the shells at $r_k$ and $r_{k+1}$ at the proper locations in $(\phi, \theta)$, then construct the interpolating polynomial that joins these two points and evaluate this polynomial at $r = r'$. This is the procedure for a linear interpolating polynomial. In practice, we ordinarily use a higher order polynomial, for example fifth degree, which requires evaluation on more spherical shells but the procedure is otherwise identical.

The total cost of evaluation per point for the B-spline model can now be made precise. If the degree of the B-spline used is *mdeg*, and the degree of the polynomial used to interpolate between shells is *ideg*, then the total cost of evaluating the model at a point is $C * (ideg + 1) * (mdeg + 1)^2$, where $C$ is a constant. Note that *ideg* is also an adjustable parameter in this model, and its value can be made smaller if we are willing to make $M$ larger, as described above for the parameter *mdeg*.

We now outline the steps in computing the coefficients for the B-spline expansion (2). For efficient and accurate computation of the coefficients, it is convenient to extend the potential function $V$ so that it is $2\pi$-periodic in both $\theta$ and $\phi$. This is done by defining

$$V_p(r, \phi, \theta) = \begin{cases} V(r, \phi + \pi, -\pi - \theta), & \text{for } -\pi \leq \theta < -\pi/2 \\ V(r, \phi, \theta), & \text{for } -\pi/2 \leq \theta \leq \pi/2 \\ V(r, \phi + \pi, \pi - \theta), & \text{for } \pi/2 < \theta \leq \pi. \end{cases}$$

for $\theta \in [-\pi, \pi]$ ($V$ is already $2\pi$-periodic in $\phi$).

There are several useful bases for splines, in addition to the "canonical" B-splines, and in this model generation step we also use the interpolating splines, $L(x)$. Interpolating splines satisfy $L(0) = 1$, and $L(n) = 0$ if $n$ is a non-zero integer. This property enables us to first write the spline expansion as

$$V(r_0, \phi, \theta) = \sum_{k=0}^{M-1} \sum_{l=0}^{M-1} A_{k,l} L\left(\frac{M\theta}{2\pi} - k\right) L\left(\frac{M\phi}{2\pi} - l\right)$$

with $A_{k,l} = V(r_0, \phi_l, \theta_k)$, where $\theta_k = 2\pi k/M$ and $\phi_l = 2\pi l/M$. To change the basis from interpolating splines (which are difficult to evaluate) to the

B-splines, all we have to do is apply an FFT to the coefficient matrix $\{A_{k,l}\}$, modify the Fourier transform by a factor, then apply the inverse FFT to obtain the B-spline coefficients in (2). As a result, the representation (2) interpolates the potential function $V(r, \phi, \theta)$, for $r = r_0$, on the equispaced grid $(2\pi k/M, 2\pi l/M)$.

Once the representation (2) for the geopotential is obtained, it is easy to build its reduced version, which is obtained by simply removing high frequencies from the model by application of multiresolution decomposition to the B-spline expansions. To describe the construction process, let us assume that $M = 2^{-j}$, where $j < 0$ is an integer, and denote the coefficients in (2) by $\{s_{k,l}^{j}\}$, to indicate that they belong to the scale $j$.

The result of applying one step of multiresolution decomposition is to compute the coefficients $\{s_{k,l}^{j+1}\}$ on the next coarser scale $(j + 1)$ (i.e. the scale corresponding to double the original step size) from the coefficients on scale $j$. From $M$ coefficients per row on scale $j$ we obtain $M/2 = 2^{-(j+1)}$ coefficients per row on scale $(j + 1)$. The steps are as follows:

1. Apply an FFT to the coefficient matrix $\{s_{k,l}^{j}\}$ to obtain the matrix $\{\hat{s}_{k,l}^{j}\}$.

2. Apply a one-dimensional decomposition in each index, i.e. first on rows, then on columns, of the matrix $\{\hat{s}_{k,l}^{j}\}$. The one-dimensional decomposition is defined as follows,

$$\hat{s}_m^{j+1} = \frac{1}{2} \left\{ \tilde{m}_0 \left( \frac{2m\pi}{M} \right) \hat{s}_m^j + \tilde{m}_0 \left( \frac{2m\pi}{M} + \pi \right) \hat{s}_{m+M}^j \right\}$$

for $m = 0, \ldots, M/2 - 1$, where the function $\tilde{m}_0$ is a $2\pi$-periodic function associated to the B-spline.

3. Apply an inverse FFT to the matrix $\{\hat{s}_{k,l}^{j+1}\}$ to obtain the coefficient matrix $\{s_{k,l}^{j+1}\}$ on the coarser scale.

Removal of the higher frequencies from the model in this manner is more stable than simply truncating them as is done, for example, in truncation of the WGS84-70 model to obtain the WGS84-41 model [11]. If desired, Steps 1-3 above can be repeated, to obtain coefficients $\{s_{k,l}^{j+2}\}$, and so on.

## 2.2 Multiwavelet Cube Model

In this model, the surface of the sphere is mapped to the surface of a cube and, instead of spheres, the concentric shells form a sequence of nested cubes. A point on the surface of a sphere is mapped to a point on the "reference cube" (which has faces perpendicular to the coordinate axes and at a distance of one unit from the origin) using the following simple algorithm.

- Input coordinates $(r, \phi, \theta)$ on the spherical surface of radius $r$.

- Compute $(x = r \sin\theta \cos\phi, \ y = r \sin\theta \sin\phi, \ z = r \cos\theta)$.

- Find $d = \max\{|x|, |y|, |z|\}$.

- Coordinates on the reference cube are $(\xi, \eta, \zeta) = (x/d, y/d, z/d)$.

Geometrically, we can think of a ray emanating from the origin, and intersecting the sphere and the reference cube each at a single point. These two points are then mapped one to the other.

We next place an equispaced rectangular grid on each face of the cube, which can then be mapped backwards onto the sphere. We note that distortion of the grid on the spherical surface caused by the curvature of the sphere is limited, and does not cause any problem near the poles.

The rectangular grid partitions each face of the cube into a number of square subdivisions, and we build a wavelet representation of the geopotential on each subdivision. Currently, the basis functions we use are the multiwavelets (see [1] and [2]), chosen because they form an orthonormal basis on a square subdivision without overlapping into adjacent subdivisions.

The scaling functions in a multiwavelet basis are classes of orthogonal polynomials, for example Legendre polynomials. Formulas for interpolating the geopotential at the Gaussian nodes within the subinterval are easily obtained using the Gaussian integration rules.

To evaluate the field between tabulated shells, we construct the Lagrangian polynomial that interpolates the values on several adjacent shells. Alternatively, we can also use expansions of multiwavelets to represent the variation in height of the gravity field.

## 2.3 Spline Cube Model

Concerning performance of the two models described thus far, two observations have been made:

1. the multiwavelet cube model has a more efficient memory access than the doubly periodic spline model, resulting in better speed for evaluation;

2. the doubly periodic spline model requires substantially fewer coefficients to achieve the same accuracy as the multiwavelet cube model.

The model described in this section has been successful in combining the best features of both these models.

To evaluate our models it is necessary to interpolate between the tabulated shells. To do this we must evaluate the two-dimensional expansions at a given point on several consecutive shells. However, the computation involves only a few coefficients on each shell, and speed is gained in memory access if these can be stored closer together.

This can be done by subdividing the surface into a number of "panels" which, taken together, cover the spherical surface. Panels for the same angles but different heights are stored contiguously in memory, which allows for faster memory access.

In this model, a partition of the spherical surface is accomplished by subdividing each spherical shell into six panels, which may be regarded as the six faces of a cube. This is done in such a way that the grid spacing for the polar regions is the same as that for the equatorial regions, and no excessive distortion of the grid on the spherical surface occurs.

To obtain six square panels, we subdivide the surface of a sphere as indicated in the following table.

|   | angle ranges | x-coordinate | y-coordinate |
|---|---|---|---|
| 1 | $-\pi \leq \phi < -\pi/2, \quad -\pi/4 \leq \theta \leq \pi/4$ | $\alpha\phi + 3$ | $\alpha\theta$ |
| 2 | $-\pi/2 \leq \phi < 0, \quad -\pi/4 \leq \theta \leq \pi/4$ | $\alpha\phi + 1$ | $\alpha\theta$ |
| 3 | $0 \leq \phi < \pi/2, \quad -\pi/4 \leq \theta \leq \pi/4$ | $\alpha\phi - 1$ | $\alpha\theta$ |
| 4 | $\pi/2 \leq \phi < \pi, \quad -\pi/4 \leq \theta \leq \pi/4$ | $\alpha\phi - 3$ | $\alpha\theta$ |
| 5 | $|\gamma| \leq 1, |\omega| \geq 1, \theta > 0$ | $\alpha\tan^{-1}(\omega) \pm 2$ | $-\alpha\sin^{-1}(\gamma)$ |
| 6 | $|\gamma| \leq 1, |\omega| \geq 1, \theta < 0$ | $\alpha\tan^{-1}(\omega) \pm 2$ | $-\alpha\sin^{-1}(\gamma)$ |

where $\alpha = 4/\pi$, $\omega = \tan\theta/\cos\phi$, and $\gamma = \cos\theta\sin\phi$. Coordinates on the face of each panel are $(x, y)$, where $-1 \leq x, y \leq 1$. The panels designated 5 and 6 contain the north and south poles, respectively. For the $x$-coordinate in panels 5 and 6, we use the minus sign if $\omega > 0$ and the plus sign if $\omega < 0$.

We note that the B-spline expansion for each panel overlaps its immediate neighbors. Thus, to use this model for the estimation problem, we would need to add a certain number of equations to ensure that the representation near the boundaries of each panel matches with that of its neighbors.

Coefficients for this model are computed in the same manner as described above for the doubly periodic spline model. After computing coefficients for a doubly periodic B-spline expansion to cover the sphere, coefficients sufficient to cover each of the first four panels are extracted and stored. The sphere is then rotated, another doubly periodic expansion is computed, then coefficients are extracted to cover the two remaining panels. The rotation is necessary to avoid excessive distortion of the grid near the poles.

We note that the gravity force field for the polar regions must be stored in rectangular coordinates. In the spherical coordinate system, the representation of a vector at one of the poles is not unique: the components of the vector can vary depending on the orientation of the spherical unit vectors. This orientation depends on the angle $\phi$, which is indeterminate at the poles. Thus, although the vector at the pole is unique, its projection onto spherical unit vectors is not.

## 2.4 Performance Results

The table below contains performance results related to the doubly periodic spline model and the spline cube model. The parameter "model order" in the far left column refers to the number of terms retained in the spherical harmonic model. The next column contains the size of the spherical harmonic model in megabytes. As can be seen, the spherical harmonic model requires very little storage space. The next pair of columns contains information relating to the doubly periodic spline model, namely the size in megabytes and speed-up factor. The speed-up factor is obtained by measuring the time required to compute the gravity vector at a large number of points, using both the spline model and the spherical harmonic model, then dividing the time for the spherical harmonic model by the time for the spline model. The final pair of columns contains size in megabytes and speed-up factor for the spline cube model. (It turns out that the multiwavelet cube model, as it is currently implemented, requires excessive memory storage, and we chose not to report performance results for this model at this time.)

8

| Model | Size of | Doubly Periodic | | Spline Cube | |
|-------|---------|------|----------|------|----------|
| Order | Sph Model | Size | Speed-up | Size | Speed-up |
| 18 | 0.003 | 4.65 | 2.3 | 10.3 | 3.6 |
| 41 | 0.013 | 33.10 | 9.0 | 27.9 | 19.5 |
| 70 | 0.038 | 76.48 | 22.9 | 70.3 | 56.1 |

The WGS84 spherical harmonic model [11] was used for these tests, with agreement to about $10^{-11}$ between spherical harmonic and spline models being maintained throughout.

Note that storage requirements for both spline models, while much larger than what is needed for the spherical harmonic models, are nevertheless quite reasonable. Furthermore, the spline models have achieved a significant speed-up in evaluation time over the spherical harmonic models. Note also that the spline cube model, which was developed during the past year, has gained better than a factor of two in speed over the previous spline model, in addition to reducing memory requirements somewhat.

# 3   Estimation of the Geopotential

Let us explain briefly why it is necessary to develop new estimation algorithms. The process of estimation (model building) of the geopotential presents several problems. First, the spatial frequency bandwidth is changing both as a function of the distance from the Earth and the location on the Earth's surface. Second, the data are typically collected on an unequally spaced grid and, as a result, the condition number of matrices involved in solving the estimation problem is usually very high.

Within the spherical harmonic representation, the problem of increasing the accuracy of the model was addressed by increasing the number of terms in the expansion. The difficulty with this approach is that spherical harmonics (being global, oscillatory functions) depend on cancellation (destructive interference) to achieve the approximation—changing even a single coefficient in the model has a global effect. In consequence, algorithms for model generation are expensive, since we have to solve systems with dense (full) matrices. It is difficult, if not impossible, to adjust the spatial frequency contents locally. In particular, there is a real problem in incorporating observations of the gravitational potential near the surface (e.g on the ground) with those obtained on satellites, apparently due to the different spectral contents of

9

the data.

Our goal has been to develop multiresolution models of the Earth's gravitational potential that do not suffer from the difficulties for use and estimation outlined above. Multiresolution models use basis functions (e.g. wavelets) with localized support in both space and spectral domains. This allows us to generate models where changes in *most* of the parameters will produce only *local* changes in the geopotential (up to any finite but arbitrary accuracy).

For a gravitational field this statement might sound strange since such fields always give rise to long range interactions; in particular, there are no negative masses and interaction appears to be global. It is easier to understand this point using the analogy with electrostatic fields which are mathematically equivalent but allow us to consider negative charges. In this case one can consider potentials consisting solely of multipole "masses" of high order for which the interaction decays very rapidly. This can occur if the masses (charges) are so arranged that the lower order moments cancel. Thus, the effects of these multipoles can be ignored beyond a relatively short distance. Wavelets can be viewed heuristically as high order multipoles.

The use of basis functions with localized support provides another benefit: the matrices for estimation of the model parameters will be sparse (up to any finite but arbitrary accuracy), which gives us a chance to develop fast algorithms for their inversion. The coefficients of these models will be estimated directly from the observed data.

## 3.1   Multiresolution QR Algorithm

Let us describe our approach to the estimation problem in more detail. As it is well known, the least-squares solution to a system of linear equations is characterized by the following

**Theorem:** *Let $A$ be a real $m \times n$ matrix and* $\mathbf{b}$ *a vector of length $m$. If* $\mathbf{x}$ *satisfies*

$$A^T A \mathbf{x} = A^T \mathbf{b}$$

*then, for any vector* $\mathbf{y}$,

$$\|\mathbf{b} - A\mathbf{x}\|_2 \leq \|\mathbf{b} - A\mathbf{y}\|_2.$$

It is typical, in practical estimation problems, for the matrix product $A^T A$ to be badly conditioned. If this is the case, or if the matrix product has a non-

10

trivial null space, then there is more than one solution to the least-squares problem. Using a standard QR factorization, it is typical to obtain that solution to the least-squares problem that minimizes the $L_2$-norm. However, for the real-world estimation problem, such solution may be meaningless. We introduce a new approach, based on a physical heuristic, namely that the solution we desire is that with the *minimum amount of detail*. That is, we attempt to minimize the high frequency content of the solution. Such procedure is feasible in a multiresolution setting, where frequency content is conveniently split across several scales, allowing us to work with each frequency range separately. The Multiresolution Rank Revealing QR algorithm we introduce is based on a standard Gramm-Schmidt QR factorization but with two new features: (1) unknowns are the wavelet coefficients, and (2) pivoting is restricted to appropriate subspaces.

As an example, consider the following system of linear equations,

$$A\mathbf{x} = \mathbf{y}, \tag{3}$$

where $A$ is a real $(m \times n)$ matrix, and we explicitly assume $m < n$. Let us express this equation in the following equivalent form,

$$\hat{A}\hat{\mathbf{x}} = \mathbf{y}, \tag{4}$$

where $\hat{A} = AW^T$, $\hat{\mathbf{x}} = W\mathbf{x}$, and $W$ denotes the wavelet transform. Since the transform is orthogonal, the product $W^T W$ is an identity. The operation $AW^T$ performs wavelet decomposition along rows of the matrix $A$, and thus the columns are effectively organized into subbands corresponding to different scales. We next construct the factorization

$$\hat{A}E = QR, \tag{5}$$

where $Q$ is an orthogonal $(m \times r)$ matrix, $R$ is an upper triangular $(r \times n)$ matrix, and $r$ is the (numerical) rank of $\hat{A}$. Note that $r \leq m$. By construction, we have $Q^T Q = I_r$, which denotes the $(r \times r)$ identity matrix. The matrix $E$ in (5) is a permutation matrix, and serves the purpose of re-ordering the columns in $\hat{A}$ so that the $r$ columns in $Q$, which form an orthonormal set, are formed from those columns in $\hat{A}$ which are largest in $l_2$-norm.

The solution to (4) is now obtained by defining

$$\hat{\mathbf{x}} = E\tilde{R}Q^T\mathbf{y}, \tag{6}$$

11

where $\tilde{R}$ is chosen to satisfy $R\tilde{R} = I_r$. Since the row dimension of $R$ is strictly less than the column dimension, there is more than one possible choice for $\tilde{R}$, and we describe our choice below. Substituting (6) into (4), we have

$$
\begin{aligned}
\hat{A}\hat{\mathbf{x}} &= (QRE^T)(E\tilde{R}Q^T)\mathbf{y} \\
&= Q(R\tilde{R})Q^T\mathbf{y} \\
&= (QQ^T)\mathbf{y}.
\end{aligned}
$$

If $r = m$, then $QQ^T$ is an identity, and we have $\mathbf{y} - \hat{A}\mathbf{x} = 0$. If $r < m$, then $QQ^T$ is a projection, and we have

$$
\|\mathbf{y} - \hat{A}\mathbf{x}\| < \epsilon
$$

if $\mathbf{y}$ lies in, or nearly in, the appropriate subspace.

Let us now describe the procedure for constructing $Q$. To begin with, we work only with the columns of averages on the coarsest scale in the transformed matrix $\hat{A}$. From among these, we choose the column with largest $l_2$-norm, and denote this column vector by $\mathbf{a}_{j_1}$, where $j_1$ is the actual column index. The first column of $Q$, denoted $\mathbf{q}_1$, is obtained as

$$
\mathbf{q}_1 = \frac{\mathbf{a}_{j_1}}{\|\mathbf{a}_{j_1}\|}.
$$

Thus, $\mathbf{q}_1^T\mathbf{q}_1 = 1$, and we now multiply all remaining columns of $\hat{A}$ by $(I - \mathbf{q}_1\mathbf{q}_1^T)$, which is projection onto the orthogonal complement of $\{\mathbf{q}_1\}$. The result of this operation is that all remaining columns (excepting $\mathbf{a}_{j_1}$) in the modified matrix $\hat{A}$ are orthogonal to $\mathbf{q}_1$.

Now repeat this step, again considering *only columns within the subband* containing averages on the coarsest scale, and choosing from among these the one with largest $l_2$-norm, which we denote by $\mathbf{a}_{j_2}$. Obtain

$$
\mathbf{q}_2 = \frac{\mathbf{a}_{j_2}}{\|\mathbf{a}_{j_2}\|},
$$

then multiply all remaining columns of $\hat{A}$ by $(I - \mathbf{q}_2\mathbf{q}_2^T)$, so that all remaining columns of $\hat{A}$ are orthogonal to $\{\mathbf{q}_1, \mathbf{q}_2\}$. We repeat this process until one of two things happens. Either we have "used up" all vectors in the subband of averages, or the remaining vectors in this subband are smaller in norm than the prescribed cutoff value. In either case, we then go to the subband

containing column vectors of wavelet coefficients on the coarsest scale, and repeat this procedure When we have either "used up" all vectors in this subband, or the vectors remaining in this subband are all smaller in norm than the prescribed cutoff, then we move to the subband which contains column vectors of wavelet coefficients on the next finer scale. This procedure is repeated until all remaining columns in $\hat{A}$, which are being overwritten at each step of the process with their projection onto the orthogonal complement of the column vectors in $Q$, are smaller in norm than the prescribed cutoff value. At this point, we have $r$ vectors in $Q$ which form an orthonormal basis (to within prescribed precision) for the column space of $\hat{A}$.

The matrix $R$ contains coefficients which represent the columns of the product $\hat{A}E$ with respect to the orthonormal basis in $Q$. In particular, the $j$th column of $R$ contains the coefficients that represent the $j$th column of $\hat{A}E$ with respect to the orthonormal basis $\{q_1, \ldots, q_r\}$, and by construction $R$ is upper triangular. To construct $\tilde{R}$, so that $R\tilde{R} = I_r$, we invert the leading $r$ columns of $R$ which, taken together, form an upper triangular $(r \times r)$ block, and thus obtain the first $r$ rows of $\tilde{R}$. We then set the remaining $(n - r)$ rows of $\tilde{R}$ to zero. This has the effect of selecting only $r$ non-zero entries in the solution vector $\hat{x}$, while setting the remaining entries to zero. The algorithm automatically selects which entries in $\hat{x}$ correspond to the most heavily weighted columns of $\hat{A}$, which for physical data should correspond to the lower frequency features of the right-hand side. We also emphasize the selection of lower frequency components by beginning the procedure with columns on the low frequency side and proceeding from lower to higher.

Figures 1–3 on the following pages compare results of Multiresolution QR and a standard QR for the following interpolation problem. In (3), the right-hand vector $\mathbf{y}$ represents values of a function, say $y(t)$, at a set of points $\{t_1, \ldots, t_m\}$. Thus, $\mathbf{y} = \{y_1, \ldots, y_m\}$, where $y_i = y(t_i)$. We build an expansion using multiwavelet scaling functions on some scale, which takes the form

$$Y(t) = \sum_{j=0}^{n-1} x_{j+1}\phi(nt - j).$$

Imposing the condition $Y(t_i) = y_i$, leads to the system of equations

$$\sum_{j=0}^{n-1} x_{j+1}\phi(nt_i - j) = y_i,$$

and comparing with (3) we see that the entry $a_{ij}$ of the matrix $A$ is given

by $\phi(nt_i - j)$, and the unknowns $\{x_1, \ldots, x_n\}$ are the coefficients of the expansion.

We choose the scale of the expansion so that the number $n$ of coefficients on the finest scale is much larger than the number $m$ of data points. However, the algorithm will select a smaller number of coefficients to represent the final solution. If the data is smooth, then the matrix $A$ will have low numerical rank at the required precision, and the final representation will be correspondingly sparse.

The next three pages contain examples which compare the results of the approached outlined above with results of the usual least squares solution method.
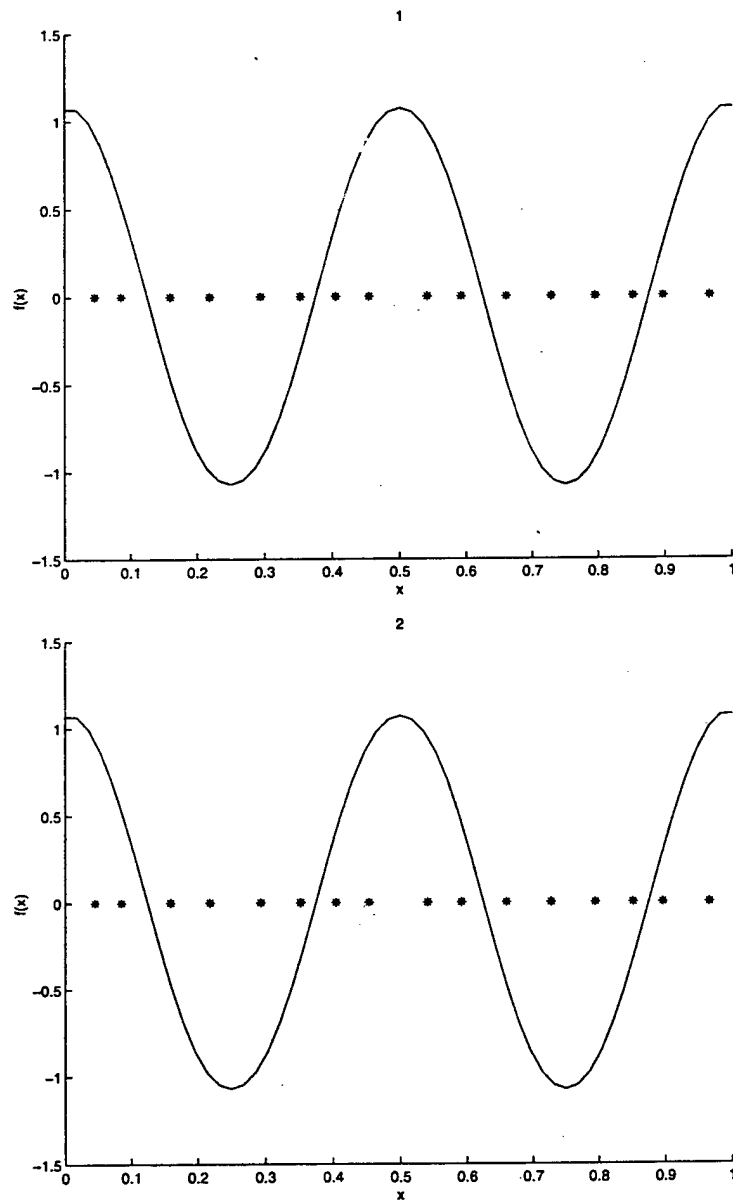
**Figure 1.** The usual QR solution (top) and multiresolution QR (bottom) for the full rank least-squares problem.
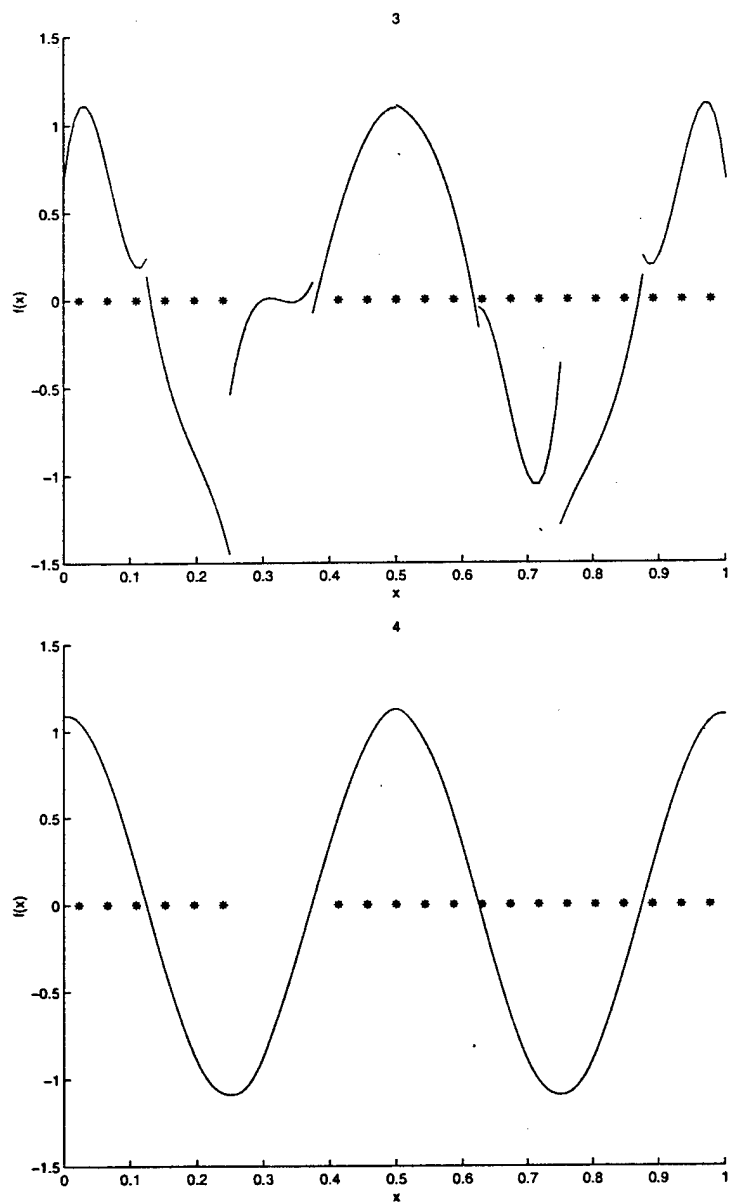
15

**Figure 2.** The usual QR solution (top) and multiresolution QR (bottom) for the least-squares problem with a null space.
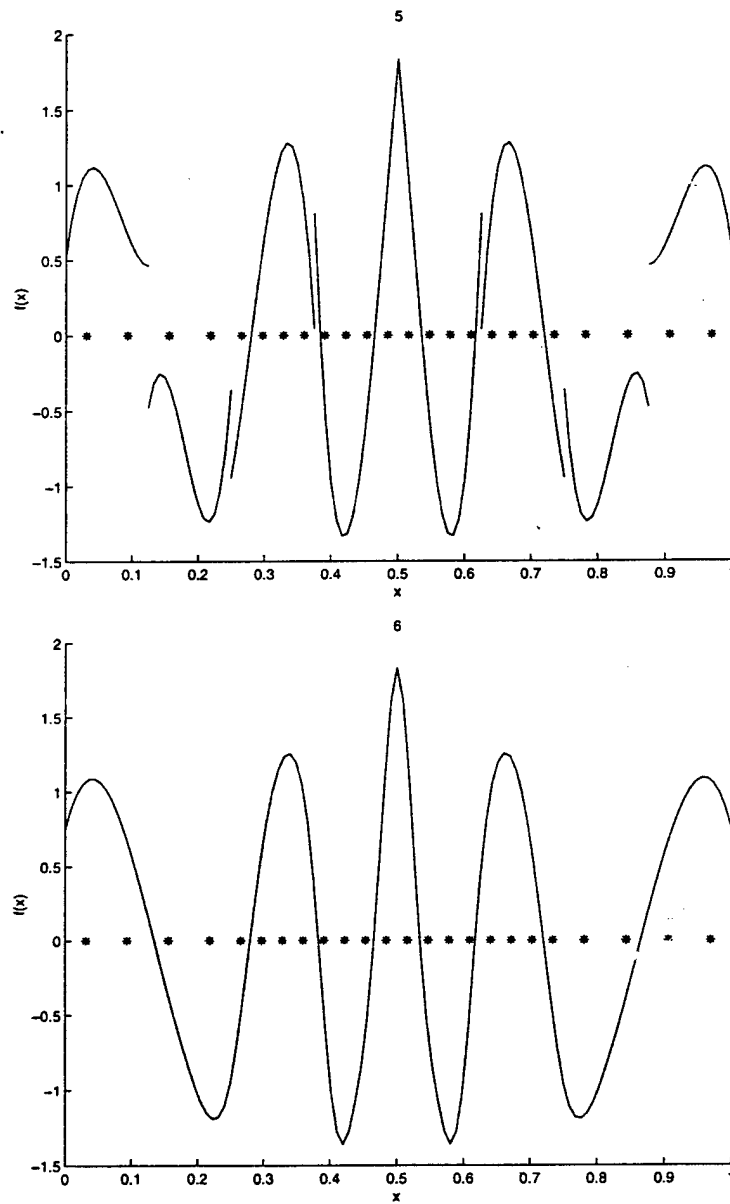
**Figure 3.** The usual QR solution (top) and multiresolution QR (bottom) for the least-squares problem with a null space.

# 4 The Next Generation of Gravity Models

The choice of basis function used to represent the gravity field is of enormous importance since this choice has the single greatest influence on the structure and performance of algorithms that will be used for evaluation and estimation of the model. Under this grant we have developed a new type of basis for estimation of gravity fields, though we have not yet developed the actual models, and we explain below the main points of the new construction. We foresee that the next generation of gravity models will use such bases in conjunction with the algorithms discussed above.

## 4.1 Optimal Bases on an Interval

Let us first provide a brief description of the prolate spheroidal wave functions (PSWFs) introduced by Slepian et. al. [20, 16].

The PSWFs are defined as the eigenfunctions of the operator $F_c$, where $F_c$ is defined by

$$F_c(\phi)(x) = \int_{-1}^{1} e^{icxt}\phi(t)dt, \tag{7}$$

where $F_c : L^2[-1,1] \to L^2[-1,1]$, and $c$ is a positive real constant (band-limit). The PSWFs satisfy

$$\lambda_j\psi_j(x) = \int_{-1}^{1} e^{icxt}\psi_j(t)\,dt, \tag{8}$$

where the eigenvalues $\lambda_j$, $j = 0, 1, 2, \ldots$, are all non-zero and simple, and are arranged so that $|\lambda_j| > |\lambda_{j+1}|$. The eigenvalues $\lambda_j$ are either real or pure imaginary depending on the parity of the eigenfunction $\psi_j$. These eigenfunctions are also eigenfunctions of the operator $Q_c = \frac{c}{2\pi}F_c^*F_c$ and satisfy

$$\mu_j\psi_j(x) = \frac{1}{\pi}\int_{-1}^{1}\frac{\sin c(x-t)}{(x-t)}\psi_j(t)\,dt, \tag{9}$$

with eigenvalues

$$\mu_j = \frac{c}{2\pi}|\lambda_j|^2, \quad j = 0, 1, 2, \ldots. \tag{10}$$

For large $c$ the first approximately $2c/\pi$ eigenvalues $\mu_j$ are close to 1. These are followed by $O(\log c)$ eigenvalues which decay exponentially fast from 1 to almost zero. The remaining eigenvalues are very close to zero.

18

In addition, there exists a strictly increasing sequence of real numbers $\eta_0 < \eta_1 < \eta_2 < \cdots$ such that the functions $\psi_j$ in (8) are eigenfunctions of the following differential operator [20],

$$L\psi_j \equiv \left(-(1-x^2)\frac{d^2}{dx^2} + 2x\frac{d}{dx} + c^2 x^2\right)\psi_j(x) = \eta_j\,\psi_j(x)\,. \qquad (11)$$

The eigenfunctions of $L$ have been known as the angular prolate spheroidal functions before the connection with (8) was discovered [20]. We note that, in the limit $c \to 0$, it follows from (11) that $\psi_j$ become the Legendre polynomials.

For any $n \geq 0$, the first $n$ functions $\psi_j$, $j = 0, \ldots, n-1$, form a Chebyshev system [14, 15]. In particular, the number of zeros of $\psi_j$ in $[-1, 1]$ is equal to $j$.

Although the functions $\psi_j$ are defined on the interval, they are easily extended to the whole line using the right hand side of (9) as the definition of the extension. The functions $\psi_j$ are orthogonal on both the interval $[-1, 1]$ and the real line $(-\infty, \infty)$, and we set

$$\int_{-1}^{1} \psi_j(x)\,\psi_l(x)\,dx = \delta_{jl}\,, \qquad (12)$$

and

$$\int_{-\infty}^{\infty} \psi_j(x)\,\psi_l(x)\,dx = \frac{1}{\mu_j}\delta_{jl}\,. \qquad (13)$$

We note that in the original papers [20, 16, 19] the functions are chosen to be orthonormal on $(-\infty, \infty)$.

The definition (8) implies that

$$e^{icxt} = \sum_{j=0}^{\infty} \lambda_j\,\psi_j(x)\psi_j(t)\,, \qquad (14)$$

and if we keep approximately $2c/\pi + K\log c$ terms in (14), where $K = K(\epsilon)$ is a constant, we obtain a close approximation to $e^{icxt}$ for any positive $\epsilon$. This is the most economical expansion of this type for the exponential.

The PSWFs have been used in signal processing for some time, especially the first function, $\psi_0(x)$, since it provides the optimal window for a given bandwidth in terms of concentration in the time-frequency domain. Yet, their use has not been wide. In the next section we describe several new developments that will provide a path for a wider use of these functions in signal processing and numerical analysis.

19

## 4.2 Generalized Gaussian Quadratures for Exponentials

The generalized Gaussian quadratures for exponentials has been developed recently [22, 6]. Within the first approach [22], the authors construct the generalized Gaussian quadratures for the prolate spheroidal wave functions using the fact that, for any $n$, the first $n$ of these functions form a Chebyshev system [14, 15]. For a given accuracy $\epsilon$ and a choice of $n$, if follows from (14) that such quadratures are also valid for exponentials. Alternatively, a new type of the generalized Gaussian quadratures for exponentials has been obtained directly [6]. These quadratures are parameterized by eigenvalues of a Toeplitz matrix which is constructed from the trigonometric moments of a positive measure. For a given accuracy $\epsilon$, selecting an eigenvalue close to $\epsilon$ yields an approximate quadrature for that accuracy. These quadratures can be used to approximate and integrate other essentially bandlimited functions such as, for example, Bessel functions or the prolate spheroidal wave functions.

Let us define the bandlimited functions with the bandlimit $c$ as a class of functions that can be represented via a linear combination of exponentials of the form $\exp(ib\,x)$ with, for example, $l^1$-bounded coefficients, where $b$ is *any* real number such that $|b| \leq c$.

It turns out that, for any accuracy $\epsilon > 0$ and any bandlimit $c > 0$, there is a set of $M$ functions, $\{\exp(ict_k\,x)\}_{k=1}^M$, where the nodes $t_k = t_k(\epsilon, c)$, $|t_k| < 1$ and the coefficients $\alpha_k = \alpha_k(b)$ are such that

$$|\exp(ib\,x) - \sum_{k=1}^M \alpha_k(b) \exp(ict_k x)| \leq \epsilon. \qquad (15)$$

The set of functions $\{\exp(ict_k\,x)\}_{k=1}^M$ can be viewed as an approximate basis.

In order to find the nodes $\{t_k\}$ in (15), we solve the following problem [6], described here in a slightly more general setting than is needed to obtain (15). Let us consider integrals of the form

$$u(x) = \int_{-1}^1 \exp(2c\,t\,x)\,d\mu(t), \qquad (16)$$

where $d\mu(t)$ is a measure. Typically, $d\mu(t) = w(t)\,dt$, where $w$ is a weight function, that is $w$ is a real, non-negative, integrable function with $\int_{-1}^1 w(\tau)d\tau > 0$. To obtain (15) the weight is defined as $w = 1$.

For a given bandlimit $2c > 0$ and accuracy $\epsilon^2 > 0$, we approximate $u(x)$ on the interval $[-1, 1]$ using the sum

$$\tilde{u}(x) = \sum_{k=1}^{M} w_k \exp\left(2c\, t_k\, x\right), \tag{17}$$

where $w_k > 0$ and $M = M(c, \epsilon^2)$, so that

$$|u(x) - \tilde{u}(x)| \leq \epsilon^2 \quad \text{for} \quad x \in [-1, 1]. \tag{18}$$

The number of terms, $M$, is optimal. Solving this problem involves finding the eigenvalues and eigenvectors of the Toeplitz matrix constructed using the values of $u(x)$ discretized at the equally spaced nodes and interpreted as the trigonometric moments of a positive measure [6].

Once the nodes are computed, the set of functions $\{\exp\left(ict_k\, x\right)\}_{k=1}^{M}$ can serve as an approximate basis on the interval $[-1, 1]$ in (15). Such bases can be organized into a hierarchical structure similar to multiwavelets. We will report these results elsewhere.

The representation in (15) retains the property of disjoint support similar to that of a multiwavelet basis. On the other hand, it requires significantly fewer terms than the representation with orthogonal polynomials. Also, one can think of the bandlimit $c$ as an analogue of the degree in the case of polynomials and, unlike in that case, there is no constraint on the bandwidth $c$. This is because the distance between the nodes is $O(1/c)$ and, thus, the quadrature nodes do not significantly concentrate near the ends of the interval as do, for example, the Legendre nodes. These properties of the representations using exponentials lead to a number of new algorithms that are being developed and will be presented elsewhere.

# 5  Spectral Deferred Corrections for Solution of Ordinary Differential Equations

This is a relatively new method for solution of ordinary differential equations [12], which shows great promise for further optimizing the computation of satellite ephemerides. The basic idea is to first obtain a crude approximation using a simple first-order method, for example an explicit Euler scheme, then to iteratively reduce (correct) the error. Methods based on this approach

are known collectively as deferred correction methods, and have been in use for some time. However, in [12] some improvement over the classical methods is introduced, namely the use of orthogonal polynomials to represent the solution, together with spectral integration, which greatly increases the stability of high-order deferred correction methods. This approach leads to methods of almost arbitrarily high order which require a relatively low number of function calls in their implementation.

We have constructed a preliminary version of a spectral deferred correction code for the orbit propagation problem, and initial tests show promise. Work is in progress towards developing a final version which is capable of replacing current operational orbit propagation codes.

# 6    Transfer of Technology

The latest version of the B-spline cube model has been transferred to Space Warfare Command (SWC) in Colorado Springs, to our point(s) of contact, Joseph Liu and Mark Storz, both of SWC. A declassified copy of currently operational code for solving ODES has been transferred to us, which allows us to make direct comparisons with new codes we are considering.

# References

[1] B Alpert. A class of bases in $L^2$ for the sparse representation of integral operators. *SIAM J. Math. Anal*, 24(1):246–262, 1993.

[2] B. Alpert, G. Beylkin, R.R. Coifman, and V. Rokhlin. Wavelet-like bases for the fast solution of second-kind integral equations. *SIAM J. Sci. Statist. Comput.*, 14(1):159–174, 1993. Technical report, Department of Computer Science, Yale University, New Haven, CT, 1990.

[3] B. Alpert, G. Beylkin, D. Gines, and L. Vozovoi. Adaptive solution of partial differential equations in multiwavelet bases. Technical Report APPM 409, Univ. of Colorado at Boulder, 1999.

[4] G. Beylkin. On the representation of operators in bases of compactly supported wavelets. *SIAM J. Numer. Anal.*, 29(6):1716–1740, 1992.

[5] G. Beylkin. On wavelet-based algorithms for solving differential equations. In John J. Benedetto and Michael W. Frazier, editors, *Wavelets: Mathematics and Applications*, pages 449–466. CRC Press, 1994.

[6] G. Beylkin and L. Monzón. On generalized Gaussian quadratures for exponentials and their applications. Technical Report APPM 452, Univ. of Colorado at Boulder, 2000. Submitted for publication.

[7] A. Cohen, I. Daubechies, B. Jawerth, and P. Vial. Multiresolution analysis, wavelets and fast algorithms on an interval. *Comptes Rendus Acad. Sc. Paris*, 1992.

[8] A. Cohen, I. Daubechies, and P. Vial. Wavelets on the interval and fast wavelet transforms. *Applied and Computational Harmonic Analysis*, 1(1):54–81, 1993.

[9] R.R. Coifman and Y. Meyer. Remarques sur l'analyse de Fourier à fenêtre. *C. R. Académie des Sciences*, 312(1):259–261, 1991.

[10] I. Daubechies. Orthonormal bases of compactly supported wavelets. *Comm. Pure Appl. Math.*, 41(7):909–996, 1988.

[11] Department of Defense World Geodetic System 1984. *Defense Mapping Agency Technical Report*, DMA TR 8350.2, 1987.

[12] A. Dutt, L. Greengard, and V. Rokhlin. Spectral deferred correction methods for ordinary differential equations. *BIT* 40(2):241–266, 2000.

[13] P. Federbush. A mass zero cluster expansion. *Communication Math. Phys.*, 81:327–340, 1981.

[14] S. Karlin and W. J. Studden. *Tchebycheff systems: With applications in analysis and statistics*. Interscience Publishers John Wiley & Sons, New York-London-Sydney, 1966. Pure and Applied Mathematics, Vol. XV.

[15] M. G. Kreĭn and A. A. Nudel'man. *The Markov moment problem and extremal problems*. American Mathematical Society, Providence, R.I., 1977. Ideas and problems of P. L. Čebyšev and A. A. Markov and their further development, Translations of Mathematical Monographs, Vol. 50.

[16] H. J. Landau and H. O. Pollak. Prolate spheroidal wave functions, Fourier analysis and uncertainty II. *Bell System Tech. J.*, 40:65–84, 1961.

[17] P.-G. Lemarié and Y. Meyer. Ondelettes et bases hilbertiennes. *Revista Mat. Iberoamericana*, 2:1–18, 1986.

[18] H. S. Malvar. Lapped Transforms for Efficient Transform/Subband Coding. *IEEE Trans. Acoust., Speech, Signal Processing*, 38(6):969–978, 1990.

[19] D. Slepian. Prolate spheroidal wave functions, Fourier analysis and uncertainty IV. Extensions to many dimensions; generalized prolate spheroidal functions. *Bell System Tech. J.*, 43:3009–3057, 1964.

[20] D. Slepian and H. O. Pollak. Prolate spheroidal wave functions, Fourier analysis and uncertainty I. *Bell System Tech. J.*, 40:43–63, 1961.

[21] J. O. Stromberg. A modified franklin system and higher-order spline systems on $\mathbf{R}^n$ as unconditional bases for Hardy spaces. In *Conference in harmonic analysis in honor of Antoni Zygmund, Wadworth math. series*, pages 475–493, 1983.

[22] H. Xiao, V. Rokhlin, and N. Yarvin. Prolate spheroidal wave functions, quadrature, and interpolation. Technical Report YALEU/DCS/RR-1199, Yale University, 2000.